Available online at www.sciencedirect.com

SCIENCE DIRECT

Biochimica et Biophysica Acta 1668 (2005) 1–9

BIOCHIMICA ET BIOPHYSICA ACTA
BBA

http://www.elsevier.com/locate/bba

The conformation of the cytoplasmic helix 8 of the CB1 cannabinoid receptor using NMR and circular dichroism

Gregory Choi, Jianxin Guo, Alexandros Makriyannis*

Center for Drug Discovery, Departments of Pharmaceutical Sciences and Molecular and Cell Biology, University of Connecticut, U-2092, 372 Fairfield Road, Storrs, CT 06269, USA

Received 30 December 2003; received in revised form 17 June 2004; accepted 27 October 2004
Available online 11 November 2004

Abstract

The cytoplasmic helix domain (fourth cytoplasmic loop, helix 8) of numerous GPCRs such as rhodopsin and the β-adrenergic receptor exhibits unique structural and functional characteristics. Computational models also predict the existence of such a structural motif within the CB1 cannabinoid receptor, another member of the G-protein coupled receptor superfamily. To gain insights into the conformational properties of this GPCR component, a peptide corresponding to helix 8 of the CB1 receptor with a small contiguous segment from transmembrane helix 7 (TM7) was chemically synthesized and its secondary structure determined by circular dichroism (CD) and solution NMR spectroscopy. Our studies in DPC and SDS micelles revealed significant α-helical structure while in an aqueous medium, the peptide exhibited a random coil configuration. The relative orientation of helix 8 within the CB1 receptor was obtained from intermolecular ^{31}P–^{1}H and ^{1}H–^{1}H NOE measurements. Our results suggest that in the presence of an amphipathic membrane environment, helix 8 assumes an alpha helical structure with an orientation parallel to the phospholipid membrane surface and perpendicular to TM7. In this model, positively charged side chains interact with the lipid headgroups while the other polar side chains face the aqueous region. The above observations may be relevant to the activation/deactivation of the CB1 receptor.

Keywords: Cannabinoid receptor; CB1; NMR; Helix 8; Circular dichroism; The fourth cytoplasmic loop

1. Introduction

The CB1 cannabinoid receptor belongs to the superfamily of G-protein coupled receptors (GPCRs). It contains an extracellular N-terminus, seven transmembrane helical segments, three intracellular and extracellular loops, and a cytoplasmic C-terminus. This receptor is widely expressed in a variety of tissues including the central nervous, cardiovascular, digestive and reproductive systems. It was shown to be involved in the modulation of a number of signaling pathways including adenylyl cyclase, Q-type Ca^{2+}, and inwardly rectifying K^{+} channels [1], and has been considered as a significant target for drug development. Conversely, its closely related subtype, the CB2 receptor, is principally expressed in cells involved in immunomodulation. It is found in high density in human spleen and tonsils [2] and, in all likelihood, is involved in signal transduction processes within the immune system [3].

Within the family of GPCRs, rhodopsin has been the target of numerous structural studies. Recently, the high-resolution crystal structure of this protein was elucidated [4], thus providing a model for other structurally related GPCRs. In the rhodopsin crystal structure, a three-turn alpha helix was identified between the C-terminal end of transmembrane helix 7 (TM7) and the beginning of the cytoplasmic C-terminus. It was designated as helix 8 and sometimes referred to as the fourth cytoplasmic loop [5–7]. Interestingly, this

Abbreviations: CD, circular dichroism; CNS, Central nervous system; DPC, Dodecylphosphocholine; SDS, sodium dodecyl sulfate; GPCRs, G-protein coupled receptors; MP-X, mastoparan-X; TM, transmembrane helix

* Corresponding author. Tel.: +1 860 486 3451; fax: +1 860 486 3089.
E-mail address: Makriyan@Uconnvm.Uconn.Edu (A. Makriyannis).

0005-2736/$ - see front matter © 2004 Elsevier B.V. All rights reserved.
doi:10.1016/j.bbamem.2004.10.011

region's structure was also predicted in various other GPCRs, including the human cannabinoid receptors, by computer modeling [8,9], sequence analysis [10,11], or by using biophysical methods [12,13]. Based on the structural data, this helix is expected to lie approximately perpendicular to the other helices and parallel to the membrane bilayer. Because of its amphipathic nature, it assumes different conformations in a solvent-dependent manner [14–16]. Also, studies with a number of different GPCRs have suggested that this segment may bind to the G-protein [17]. Specifically, a synthetic peptide fragment possessing the helix 8 sequence was shown to compete with the intact receptor for G-protein binding [12,18].

In this study, we have synthesized a I397–G418 peptide, which corresponds to a CB1 receptor segment comprising the entire intracellular helix 8 region in addition to a small segment from TM7. Truncated proteins or protein fragments are known to have defined secondary structures [19,20]. The secondary structure of this peptide was determined by NMR and circular dichroism (CD) under different solvent environments, including water, SDS and DPC micelles. In an aqueous solution, the peptide was found to assume a random coil conformation, while in membrane-like environment it exhibited a stable α-helical secondary structure. Additionally, ^{1}H–^{31}P and ^{1}H–^{1}H NOE experiments have provided evidence that the peptide orients with its cationic arginine residues facing the membrane surface. The aromatic side chain protons of F409 are found to be in contact with the headgroup as well as part of the acyl chain of DPC. Our findings provide the basis for a hypothesis according to which helix 8 plays a significant role in the function and regulation of the CB1 receptor as well as other GPCRs.

2. Experimental procedures

2.1. Peptide synthesis

Peptide I397–G418 was synthesized by solid-state synthesis on an Applied Biosystems 433A peptide synthesizer, using FastMOC chemistry on HMP resin at room temperature. HBTU was used for activation and the resin was washed with NMP. The peptide was purified by HPLC and structurally confirmed by mass spectral analysis.

2.2. Preparation of DPC and SDS micelles

Fully deuterated dodecylphosphocholine (DPC) and sodium dodecyl sulfate (SDS) were obtained from Isotec and Cambridge Isotopes, respectively, while unlabelled DPC was from Avanti Polar Lipid, Inc. DPC was first dissolved in chloroform and dried in a round bottom flask until a thin film was formed. Distilled, deionized water (600 μl) preadjusted to pH 5.5 was then added and the mixture sonicated in an ultrasonication bath to obtain a clear solution. The peptide was dissolved separately in distilled, deionized water at pH 5.5 (200 μl) and added gradually to the DPC solution to produce a micelle/peptide mixture which was then subjected to further ultrasonication (5×3 min) with a 1-min interval between each sonication. SDS micelles were prepared in a similar fashion. In both cases, the molar ratio between peptide and micelles was kept at 1:1. The aggregation numbers of both detergents are about 67, thus a molar ratio of 1:70 between peptide and detergent was used.

2.3. Circular dichroism

CD spectra were recorded on a Jasco J-715 spectrometer from 190 to 260 nm in 0.5-nm steps and a 1-s integration time at 25 °C. Measurements were carried out in cuvettes of 0.2-cm path length at a peptide concentration of 100 μM in water (pH 5.5) or in DPC micelles at the same pH. Spectra were plotted as the mean residue molar ellipticity, and quantification of the secondary components was carried out by analogy with the computed spectra of model systems [21].

2.4. NMR spectroscopy

A peptide sample in DPC micelles consisted of 2.4 mM peptide and 168.0 mM deuterated DPC in 0.6 ml of H_2O/D_2O (90%/10%, v/v) at pH 5.5. In the case of peptide sample with protonated DPC, 16.80 mM of fully protonated DPC was added. In the aqueous sample, 2.4 mM peptide was dissolved in 0.6-ml H_2O/D_2O (90%/10%, v/v) at pH 5.5. All spectra were recorded at 285 K (12°C) on a Bruker DMX-500 spectrometer operating at proton frequencies of 500 MHz. In experiments used for spectral assignments, the sweep width was 6265 Hz and spectra were referenced to an external sample of DSS in H_2O/D_2O (90%/10%, v/v) at pH 5.5. Water suppression was accomplished by a WATERGATE gradient pulse as well as by selective saturation of water during the relaxation delay of all NMR experiments and during the mixing period of the pure absorption phase of NOESY experiments [22]. The 2D NOESY spectra were obtained with a mixing time of 150 ms for water samples. For DPC micelle samples, spectra were obtained using mixing times of 25, 50, 100, 150, 200, 250, 300 and 450 ms. NOEs were found to increase linearly up to a mixing time of 250 ms. Based on these results, a 150-ms mixing time was selected for the NOE assignments of the DPC micelle samples. TOCSY spectra were acquired using a standard MLEV 17 pulse sequence, with a 100-ms spin-lock period. For the ^{1}H–^{31}P Heteronuclear NOESY spectrum of the peptide in DPC micelles, a mixing time of 400 ms was used to determine the NOE assignments.

All 2D experiments used for peak assignments were recorded using time-proportional phase incrementation (TPPI) for quadrature detection in F1, with 128 transients, 512 complex points in the t1 dimension and 2048 points in the t2 dimension. Data sets were processed on a SGI Indy workstation utilizing XWinNMR software from Bruker.

2.5. Energy minimization and molecular dynamics

Sybyl 6.6 (Tripos) was used for all structural calculations while the Kollman-All-Atom force field and Kollman charges were used within Sybyl 6.6. A combination of simulated annealing, constraint-based restrained molecular dynamics (DYANA) [23], and energy minimization was used to generate the final structures. First, a nonstructured model for the peptide was built via the Biopolymer module and NOE constraints generated from the NMR-Triad module were added. DYANA was first used to calculate the most probable structures. The 10 best structures with the lowest target functions were selected and subjected to 50 cycles of simulated annealing, to obtain a folded peptide structure that was consistent with the available experimental distance constraints. In each cycle the construct was heated to 1000 K for 1000 fs and then cooled to 300 K for 1500 fs. The final structures were subsequently minimized until the lowest possible energy was reached. All calculations were performed on an SGI Fuel workstation with a 600-MHz MIPS R14000 processor.

3. Results

3.1. CD experiments

CD measurements of the I397–G418 peptide were performed in different solvents (Fig. 1). In pure water the peptide exhibited mainly a random coil conformation with only 10% α-helical characteristics. In contrast, the CD spectrum of the peptide dissolved in 10 mM DPC micelles indicated that the peptide was 65% α-helical. The peptide spectrum in SDS was not measured since the absorption of SDS interfered with the spectral analysis.

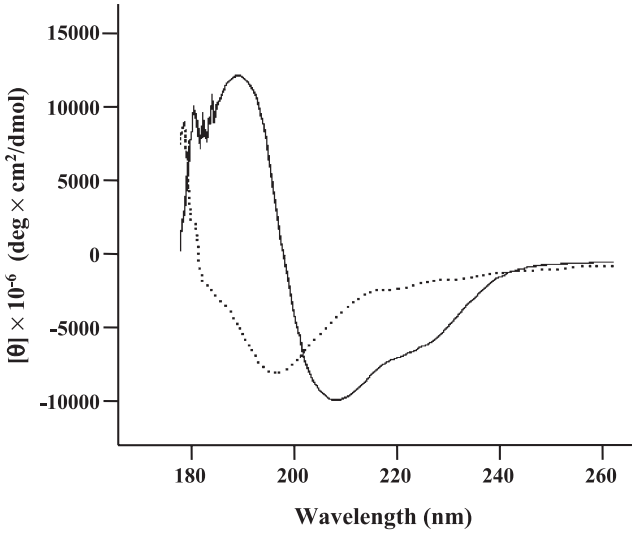

Fig. 1. CD spectra of the peptide I397–G418. CD spectra of 100 μM peptide in the absence (dotted line) and presence (solid line) of 10 mM of DPC micelles at pH 5.5 and 25 °C. The measurements were carried out in cuvettes of 0.2-cm path length. Spectra were recorded from 190 to 260 nm in 0.5-nm steps at 1-s integration time. Ellipticity was recorded as mean residue molar ellipticity as calculated by the instrument software provided. Quantification of the secondary components was done by comparison with computed spectra of model systems [21]. In DPC micelles, peptide I397–G418 exhibits a predominantly (65%) classical α-helical CD profile, in contrast to the random coil profile (below 10% α-helix) shown in the absence of DPC.

3.2. ^{1}H NMR experiments

^{1}H NMR was performed on the peptide in aqueous solution, and in the presence of DPC at a molar ratio of 1:70 peptide to DPC. Under aqueous conditions, no secondary structural features were observed based on the 2D NOESY experiment, only sequential connectivities were found (data not shown). The NOESY spectra of the peptide in SDS and DPC micelles were in agreement and both indicated an α-helical conformation with the typical pattern of NN (i, i+1), αN (i, i+3), and αβ (i, i+3) cross-peaks. Importantly, the cross-peaks confirm a high degree of α-helical structure from residue 6 to 16, which correspond to S402–M412 in the CB1 receptor. Such results agree with the highly helical secondary structure observed in the CD measurements. The spectrum of N–N connectivities, based on the observed NOEs, is shown in Fig. 2. All the detected cross-peaks in the NOESY experiment are summarized in Fig. 3 while the assignments of the chemical shifts from samples of DPC micelles are listed in Table 1. There are a total of 37 observed cross-peaks where 25 are short-range NOEs (i+1), 10 are medium- to long-range (i.e., i+2 and i+3) inter-residue NOEs, and two belong to very-long-range (i+4) inter-residue NOEs. Most of these occur between S402 and S411. In addition, there are three inter-residue NOEs from side chain–side chain interactions with structural significance, which will be discussed later. These include the γCH_2 of R406 and the δ aromatic protons of F409 (1.52/6.72 ppm), the δ aromatic protons of F409 and δCH_2 of R410 (6.72/3.00 ppm), δCH_2 of R406 and γCH_2 of H407 (2.91/3.17 ppm).

3.3. Computed secondary structure

The secondary structures of the I397–G418 peptide in DPC micelles were obtained from NOE distance-restrained molecular dynamics. NOESY spectra were assigned and NOE intensities were measured in terms of peak volume. NOE cross-peaks were divided into three classes corresponding to strong, medium and weak intensities and were assigned inter-hydrogen distances of 1.5–2.5, 1.5–3.7 and 3.0–5.0 Å, respectively. Pseudoatoms were applied to the methylene and methyl hydrogens that were not stereospecifically distinguishable. The computer modeling program Sybyl 6.6 (Tripos) was used to build the initial structure of the I397–G418 peptide. Its structure in DPC micelles is shown in Fig. 4, displaying a three-turn helix within the middle portion of the peptide. Noticeably, based on this model, the cationic hydrophilic side chains of histidine, arginine and lysine are located on the same side of

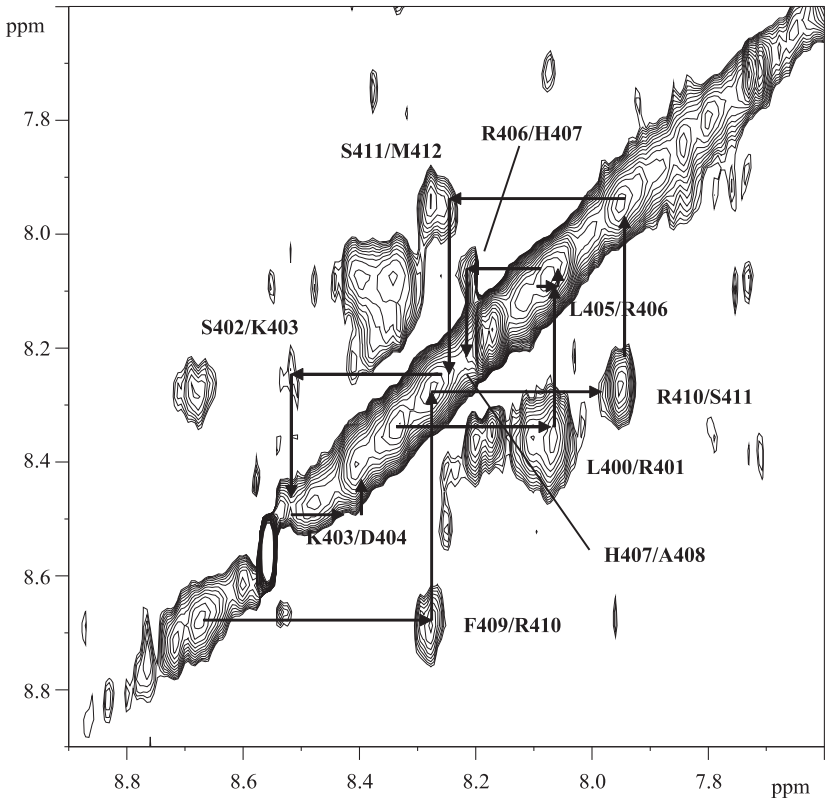

Fig. 2. 2D NOESY spectrum of the peptide I397–G418 in DPC micelles. Amide resonance region showing the $N_{\alpha}H_{i}$–$N_{\alpha}H_{i+1}$ and ^{1}H NMR cross-peaks of the NOESY spectrum at pH 5.5 and 12 °C. These cross-peaks confirm a high degree of α-helical structure from residue 6 to 16, which is equivalent to S402–M412 in the CB1 receptor. The results agree with the CD measurements described in Fig. 1.

the helix while other polar or anionic groups are on the other side. Our experimental data indicate a break of the helical structure at residues 4 and 5 corresponding to L400 and R401 in CB1 and suggest a higher degree of flexibility in this peptide region. This feature becomes more apparent when comparing the 10 lowest energy structures calculated from the NMR data. Our results show that residues I397 to L400 can be assigned to the cytoplasmic end of TM7 and that R401 constitutes a discontinuity between TM7 and the beginning of helix 8 from S403. The flexible nature of R401 is in agreement with the rhodopsin crystal and computer model structures [9,10]. Thus, we conclude that peptide

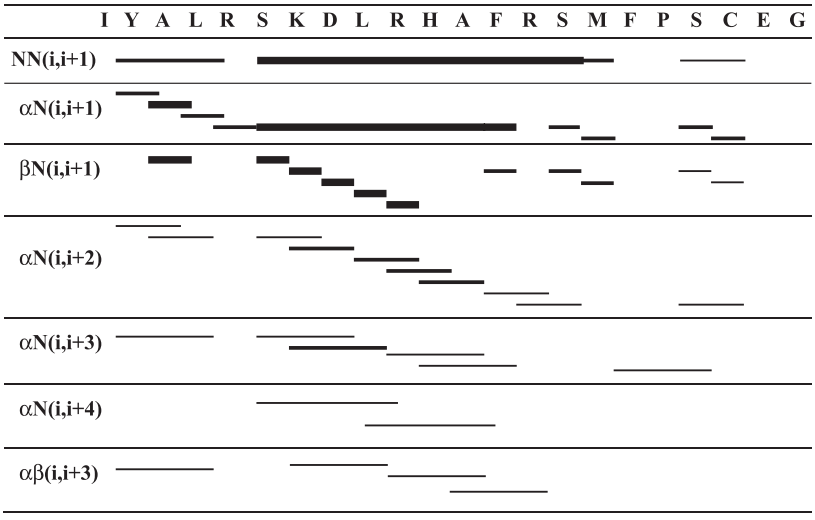

Fig. 3. Summary of ^{1}H–^{1}H NOE connectivities for the peptide I397–G418 in DPC micelles. The diagrammed NOE connectivities indicate an α-helical conformation with the typical pattern of NN (*i*, *i*+1), αN (*i*, *i*+3), and αβ (*i*, *i*+3) cross-peaks. There are 10 medium- to long-range (i.e., *i*+2 and *i*+3) inter-residue NOEs, and two long-range (*i*+4) inter-residue NOEs. Most of these NOEs occur between S402 and S411. A total of 25 short-range NOEs (*i*+1) are found. In addition, there are eight NN (*i*, *i*+1) NOEs found between S402 and S411, as shown in Fig. 2.

Table 1
Chemical shifts from peptide I397–G418 of CB1 in DPC micelles

Residue	Amide NH	αCH	βCH	χCH	Others
397. ILE(I)	8.07	3.81	1.45, 1.64	1.33	1.07
398. TYR(Y)	8.35	4.37	2.89, 2.98		6.73(δCH), 7.03(εCH, ζCH)
399. ALA(A)	8.28	4.18	1.27		
400. LEU(L)	8.32	3.87	1.73, 1.83	1.07	0.87
401. ARG(R)	8.05	4.10	1.26, 1.61	1.34	2.88(δCH), 6.44, 7.12(NH)
402. SER(S)	8.26	4.21	2.90, 2.99	3.85	
403. LYS(K)	8.53	4.21	1.77	1.44	
404. ASP(D)	8.40	4.42	2.27, 2.87		
405. LEU(L)	7.94	4.21	1.59, 1.73	1.28	0.87
406. ARG(R)	8.07	3.78	1.94	1.52	2.91(δCH), 6.60, 6.97(NH)
407. HIS(H)	8.20	4.06	2.88	3.17	7.71(2H), 8.62(4H)
408. ALA(A)	8.17	3.87	1.08		
409. PHE(F)	8.68	4.38	2.88		6.72(δCH), 7.02(εCH, ζCH)
410. ARG(R)	8.27	3.65	1.65	1.38	3.00(δCH), 6.68, 7.22(NH)
411. SER(S)	7.96	4.20	3.88	3.98	
412. MET(M)	8.26	4.33	2.03	1.78	
413. PHE(F)	8.38	4.10	2.85		6.74(δCH), 6.97(εCH, ζCH)
414. PRO(P)	N.A.	4.30	1.75	1.96	3.42(δCH)
415. SER(S)	8.11	4.37	3.87	3.99	
416. CYS(C)	7.99	3.91	3.00		
417. GLU(E)	8.06	4.43	1.91	2.22	
418. GLY(G)	8.40	3.89			

I397–G418 forms an α-helical structure in a membrane-like amphipathic environment. This structure is interrupted at R401, which acts as a hinge for the remaining peptide residues at the distal portion of the helix. Conversely, in an aqueous environment, the peptide remains highly flexible with no secondary structure.

3.4. 2D ^{1}H–^{31}P heteronuclear NOESY of the peptide in DPC micelles

Two cross-peaks were observed due to the NH arginine side chain protons and the ^{31}P of the phosphate group in DPC (Fig. 5). The more intense cross-peak at δ(^{1}H) 6.68 ppm indicates a strong dipolar interaction between the headgroup phosphorus of DPC and the NH proton from the side chain of R410. The weaker cross-peak at δ(^{1}H) 6.60 ppm corresponds to an NOE between the DPC phosphorus and the side chain NH proton of R406. The above observations, in combination with the established secondary helical structure of this segment of the peptide, can be used as structural information regarding the peptide orientation in

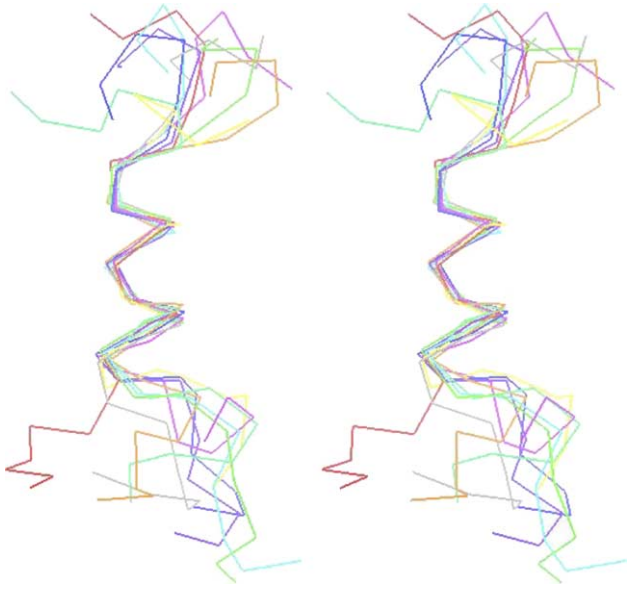

Fig. 4. Stereo-view of the secondary structure of peptide I397–G418. The structure exhibits a three-turn α-helical conformation, with hydrophobic residues on one side of the helix and cationic residues on the other. RMSD was 0.75 when the α-carbons among 10 overlapped structures are compared. The superposition consists of the 10 lowest energy structures calculated from the NMR data. High flexibility at the L400 and R401 residues causes the overlapping of I397 to R401 to be less consistent in comparison to the rest of the peptide. DYANA was first used to calculate the most probable structures based on the NOE distance constraints. The 10 best structures were subjected to further simulated annealing of 50 cycles to fold a structure that was consistent with the available experimental distance constraints. In each cycle, the construct was heated to 1000 K for 1000 fs and then cooled to 300 K for 1500 fs. The final structures were minimized until the lowest possible energy was reached. The Kollman-All-Atom force field and Kollman charges were used within Sybyl 6.6.

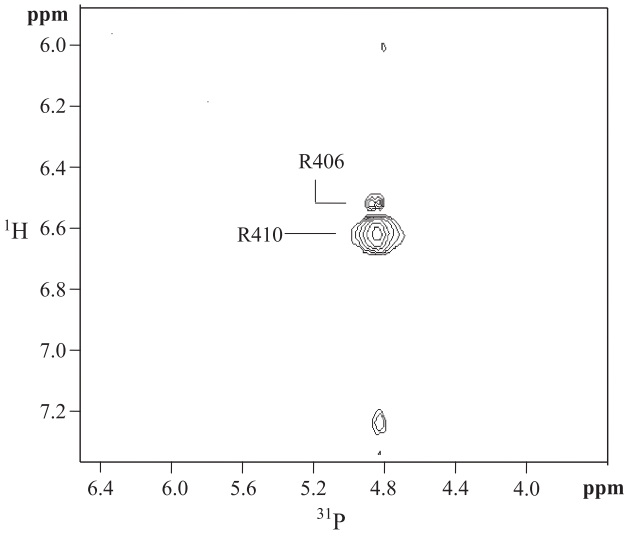

Fig. 5. 2D ^{31}P–^{1}H Heteronuclear NOESY spectrum of the peptide I397–G418 in DPC micelles. Amide resonance region showing a major cross-peak of the NOESY spectrum of the peptide in DPC micelles at pH 5.5 and 12 °C. A mixing time of 400 ms was used and the ^{31}P chemical shifts were referenced externally with phosphoric acid (H_3PO_4). The cross-peaks indicate a high degree of interaction of the phosphorus headgroup of DPC with R410 and a weaker interaction with R406.

the amphipathic lipid medium. R410 is located in the third turn of the helix, while R406 is expected to be in the second turn and roughly in the midpoint of the helix. Although the two cationic residues are not fully aligned with each other with R406 being in a position slightly less exposed to the lipid membrane surface, R406 is on the same side of the helix as R410. Thus, the NOE data suggest an interaction between the two cationic arginine residues on one side of the helix with the polar micelle surface. The observed differences in the intensities of these ^{1}H–^{31}P NOE interactions may reflect a more optimal orientation of R410 guanidinium group with regard to the micelle surface compared to its R406 counterpart. The heteronuclear NOESY experiment is congruent with the inter-residue ^{1}H side chain–side chain NOE results described earlier, indicating that L405 is adjacent to R406 and F409, with the latter two separated by one helix turn and are situated on the same side of the helix facing the amphipathic micelle surface.

3.5. 2D ^{1}H NOESY spectrum of the peptide in 10% protonated DPC micelles

In an attempt to observe possible intermolecular ^{1}H–^{1}H NOEs between the DPC headgroup and nearby residues, we used a model membrane sample in which 10% of the DPC was fully protonated (20.0 mM) while the remaining 90% had its acyl chains and headgroup fully deuterated. The NOESY spectrum (Fig. 6) was compared to that from a sample made up entirely of fully deuterated DPC/peptide micelles under identical experimental conditions. The major chemical shifts from DPC are listed in Table 2, and are in agreement with previous work [24,25]. Comparison of the two spectra has identified several new NOE cross-peaks (Table 3). These include cross-peaks between 4.19 ppm and 6.72, 7.02 and 7.96 ppm which are due to the CH_2 protons [$(CH_3)_3N^+$-C**H$_2$**-CH_2-O-PO_3-] of the DPC headgroup interacting with the δ and ε protons of the aromatic side chain of F409, and with the

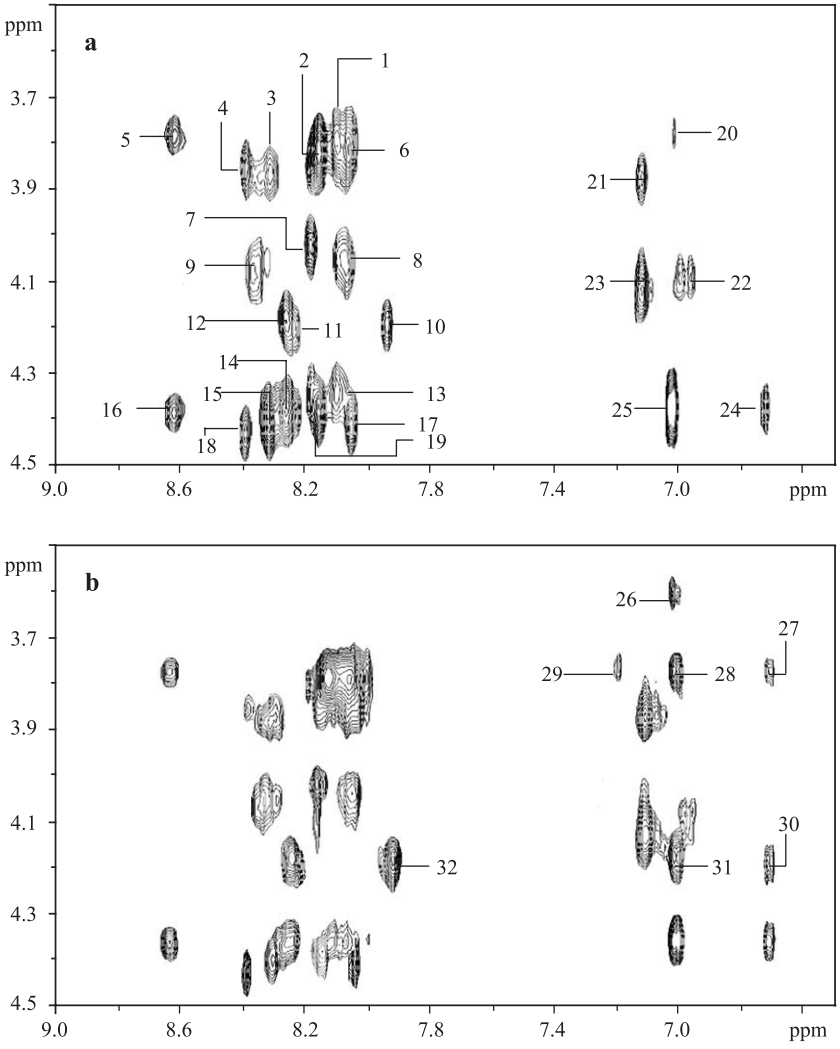

Fig. 6. 2D ^{1}H–^{1}H intermolecular NOESY spectrum of the peptide I397–G418 in DPC micelles. Amide resonance region of the peptide in (a) deuterated DPC micelles; (b) 10% fully protonated DPC and 90% deuterated DPC micelles. The labeled cross-peaks (#1–#25) in panel a are common in the two spectra and the new NOE peaks (#26–#32) in panel b reveals intermolecular interactions between DPC and peptide residues. The assignments of all numbered cross-peaks are tabulated in Table 3. The minor differences at the peptide amide region (7.9–8.7 ppm, *x*-axis) are artifacts due to the strong presence of DPC signals in spectrum *b*.

Table 2
Major ^{1}H chemical shifts (ppm) for DPC

0.79	$C\mathbf{H}_3$-$(CH_2)_9$-CH_2-CH_2-PO_4-CH_2-CH_2-$N(CH_3)_3^+$
1.20–1.26	CH_3-$(C\mathbf{H}_2)_9$-CH_2-CH_2-PO_4-CH_2-CH_2-$N(CH_3)_3^+$
1.60	CH_3-$(CH_2)_9$-$C\mathbf{H}_2$-CH_2-PO_4-CH_2-CH_2-$N(CH_3)_3^+$
3.78	CH_3-$(CH_2)_9$-CH_2-$C\mathbf{H}_2$-PO_4-CH_2-CH_2-$N(CH_3)_3^+$
3.60	CH_3-$(CH_2)_9$-CH_2-CH_2-PO_4-$C\mathbf{H}_2$-CH_2-$N(CH_3)_3^+$
4.19	CH_3-$(CH_2)_9$-CH_2-CH_2-PO_4-CH_2-$C\mathbf{H}_2$-$N(CH_3)_3^+$

L405 NH amide proton. Also, the cross-peak of 3.60/7.02 ppm corresponds to the CH_2 protons of the DPC headgroup [$(CH_3)_3N^+$-CH_2-$C\mathbf{H}_2$-O-PO_3-] and the F409 ε aromatic side chain protons. Additional cross-peaks are found between the alpha methylene protons of the DPC [$(CH_3)_3N^+$-CH_2-CH_2-O_3P-O-$C\mathbf{H}_2$-$(CH_2)_{10}$-CH_3] and the aromatic δ, ε side chain proton of F409 (3.78/6.72 and 7.02 ppm). Notably, the NOEs of the F409 ε side chain proton are more intense than those from its δ counterpart, indicating that the εCHs of F409 have stronger interactions with the DPC micelles than the δCHs.

Table 3

No.	Chemical shift (ppm)	Assignments
(a) ^{1}H–^{1}H NOE cross-peaks of peptide I397–G418 in DPC micelles		
1	3.78/8.07	R406 αCH-NH
2	3.87/8.17	A408 αCH-NH
3	3.87/8.32	L400 αCH-NH
4	3.89/8.40	G418 αCH-NH
5	3.78/8.68	(*i*+3) R406 αCH-F409 NH
6	3.81/8.07	I397 αCH-NH
7	4.06/8.20	H407 αCH-NH
8	4.10/8.05	R401 αCH-NH
9	4.10/8.38	F413 αCH-NH
10	4.21/7.94, 4.20/7.96	L405 αCH-NH, S411 αCH-NH
11	4.21/8.26	S402 αCH-NH
12	4.18/8.28	A399 αCH-NH
13	4.37/8.11	S415 αCH-NH
14	4.33/8.26	M412 αCH-NH
15	4.37/8.35	Y398 αCH-NH
16	4.38/8.68	F409 αCH-NH
17	4.43/8.06	E417 αCH-NH
18	4.42/8.40	D404 αCH-NH
19	4.38/8.17	(*i*−1) F409 αCH-A408 NH
20	3.78/7.02	(*i*+3) R406 αCH-F409 εCH
21	3.87/7.12	(*i*+1) L400 αCH-R401 NH side chain
22	4.10/6.97	F413 αCH-εCH
23	4.10/7.12	R401 αCH-NH side chain
24	4.38/6.72	F409 αCH-δCH
25	4.38/7.02	F409 αCH-εCH
(b) Intermolecular ^{1}H–^{1}H NOEs between DPC and peptide residues		
26	3.60/7.02	CH_3-$(CH_2)_{10}$-CH_2-O_3P-O-$C\mathbf{H}_2$-CH_2-$N(CH_3)_3^+$/F409 εCH
27	3.78/6.72	CH_3-$(CH_2)_{10}$-$C\mathbf{H}_2$-O-PO_3-CH_2-CH_2-$N(CH_3)_3^+$/F409 δCH
28	3.78/7.02	CH_3-$(CH_2)_{10}$-$C\mathbf{H}_2$-O-PO_3-CH_2-CH_2-$N(CH_3)_3^+$/F409 εCH
29	3.78/7.22	CH_3-$(CH_2)_{10}$-$C\mathbf{H}_2$-O-PO_3-CH_2-CH_2-$N(CH_3)_3^+$/R410 NH side chain
30	4.19/6.72	CH_3-$(CH_2)_{10}$-CH_2-O_3P-O-CH_2-$C\mathbf{H}_2$-$N(CH_3)_3^+$/F409 δCH
31	4.19/7.02	CH_3-$(CH_2)_{10}$-CH_2-O_3P-O-CH_2-$C\mathbf{H}_2$-$N(CH_3)_3^+$/F409 εCH
32	4.19/7.94	CH_3-$(CH_2)_{10}$-CH_2-O_3P-O-CH_2-$C\mathbf{H}_2$-$N(CH_3)_3^+$/L405 NH

4. Discussion

The 2D ^{1}H NMR data provide evidence that the peptide being studied lacks secondary structural features in an aqueous medium but acquires a clear helical structure when introduced in an amphipathic membrane-like medium. Analysis of the spectra demonstrated the existence of a three-turn helical structure (Fig. 7a and b) within peptide I397–G418 in a micellar solution. In addition to the ^{1}H–^{31}P interactions between R406, R410 side chain protons and the phosphate group of the phospholipid micelles, NOE experiments from the protonated DPC sample provided evidence for ^{1}H–^{1}H dipolar interactions between L405, F409, R410 and the headgroup and interface region of DPC. All of the

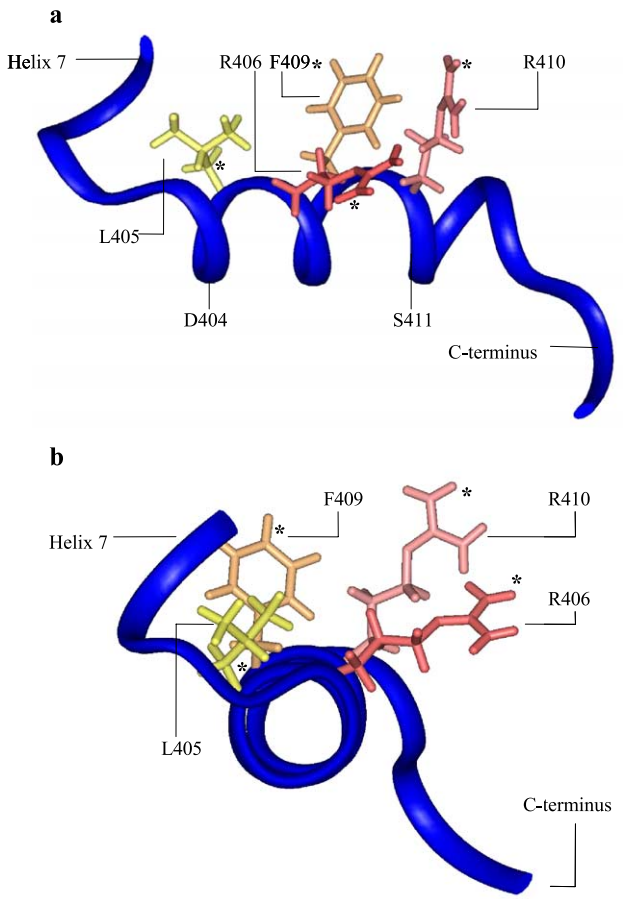

Fig. 7. Illustrations of helix 8 orientation. (a) Based on the secondary structure, L405, F409 and R410 and, to a less extent, R406 are found to be located on the same side of the helix. (b) Secondary structure of helix 8 viewed from the longitudinal axis. * Indicates the protons involved in the intermolecular NOE interaction with the DPC, namely, the amide NH of L405, the side chain NH of R406, the aromatic δ and ε CH of F409 and side chain NH of R410. The positively charged R residues are located on one side of the helix and the negatively charged D and polar S residues are on the other side.

above residues were shown to be situated on the same side of the helix as illustrated in Fig. 7. The data are congruent with a model in which the helical component of the peptide is anchored at the phospholipid micellar surface through an interaction between the cationic R406 and R410 residues with the corresponding anionic phosphate groups of DPC. The weaker interaction of R406 with the phosphate group indicates a suboptimal alignment of this residue with regard to the anionic sites of the micellar surface. According to this model, the anionic D404 residue as well as the polar uncharged S411 are situated on the opposite side of the peptide's helical structure facing the aqueous medium. When interpreted in terms of a CB1 helix 8 structure, our model suggests that this I397 to G418 region of CB1 adopts a helical structure when introduced into a membrane like environment. Our data do not provide conclusive evidence on the relative orientation of the helix 8 peptide with regard to TM7 as they are limited by the fact that only a small segment of TM7 is encompassed in the peptide being studied. However, by analogy with the rhodopsin structure, we can speculate that helix 8 is orthogonal with TM7 and lies parallel with the intracellular surface of the membrane bilayer with which it interacts through its cationic peptide residues. On the other hand, the cytoplasmic face of the helix encompasses other non-cationic polar residues including D404 and S411 while the junction between TM7 and helix 8 occurs at the R401 residue which exhibits a high degree of flexibility.

Sequence analysis within the GPCR family reveals that the N-terminus of helix 8 is highly conserved [11], and accumulating evidence indicates that it may be responsible for G-protein activation [11,18,26–28]. Also, it has already been demonstrated that the helix 8 fragment of CB1 binds to G-protein and successfully competes with the CB1 receptor for this binding [12,13]. Intriguingly, mastoparan-X (MP-X), a cationic α-helical peptide that exists in wasp venom [29] and shares structural similarities with helix 8, was shown to bind to G-protein and trigger the corresponding physiological responses [30,31]. Based on our results, it could be argued that MP-X may mimic the helix 8 region of GPCRs by binding to the receptor-binding domain of G-proteins [32].

The amphipathic nature of helix 8 and other structurally similar peptides suggests some interesting structural and functional considerations regarding receptor activation [29,30]. We may speculate that helix 8 of the CB1 receptor aligns itself parallel to the bilayer surface with its positively charged side chains interacting with the anionic phospholipid headgroups. The relatively short linear NOE build-up periods due to peptide protons within these micellar preparations when compared to the same peptide in aqueous solution support our interpretation that the peptide is anchored at the surface of the micelles. The DPC lipid headgroup interactions with residues L405, R406, F409 and R410 further reinforce our peptide/membrane model. These solvent-dependent conformational changes may play a role in the regulation and function of CB1 receptor. Specifically, this peptide/membrane interaction might serve as a regulatory mechanism according to which the amphipathic helix functions as a reversible membrane anchor. Such hypothesis is likely to be applicable to the GPCR superfamily as a whole, since the solvent-dependent conformational differences for helix 8 peptides have also been reported in other GPCRs [12–16]. A similar hypothesis has recently been proposed in an X-ray structural study of beta-arrestin [33]. In addition, Abdulaev and Ridge [34] reported that the cytoplasmic end of TM7 in rhodopsin was found to be exposed to the aqueous environment during receptor activation. Such a result suggested that helix 8 may also have become exposed to the hydrophilic cytoplasm upon receptor activation. The flexibility of helix 8 in an aqueous environment may favor its subsequent binding to the G-protein by making it more accessible for such an interaction [35]. Alternatively, this surface anchoring mechanism of helix 8 to the bilayer may serve as a mechanism aimed at concealing the potential G-protein binding regions when the receptor is in its inactive conformation. Once the receptor is activated, helix 8 might become unanchored, and structural features such as the arrestin binding site or the phosphorylation site at the C terminus may be revealed.

Our findings are congruent with other structural studies on various GPCRs, including the closely related CB2 receptor. We suggest that these observations may provide a possible common mechanism for G-protein activation.

Acknowledgement

This work was supported by grants from the National Institute on Drug Abuse (DA 3801, DA 9158, DA 7312). Helpful discussions with Professor De-Ping Yang at the College of the Holy Cross and Dr. Xiaoyu Tian at our Center for Drug Discovery are highly appreciated. We also thank Dr. Judith Landin for the peptide synthesis.

References

[1] S. Munro, K.L. Thomas, M. Abu-Shaar, Nature 365 (1993) 61–65.
[2] K. Mackie, B. Hille, Proc. Natl. Acad. Sci. U. S. A. 89 (1992) 3825–3829.
[3] S. Galiegue, S. Mary, J. Marchand, D. Dussossoy, D. Carriere, P. Carayon, M. Bouaboula, D. Shire, G. Le Fur, P. Casellas, Eur. J. Biochem. 232 (1995) 54–61.
[4] K. Palczewski, T. Kumasaka, T. Hori, C.A. Behnke, H. Motoshima, B.A. Fox, I. Le Trong, D.C. Teller, T. Okada, R.E. Stenkamp, M. Yamamoto, M. Miyano, Science 289 (2000) 739–745.
[5] A. Ovchinnikov Yu, N.G. Abdulaev, A.S. Bogachuk, FEBS Lett. 230 (1988) 1–5.
[6] M.E. Kennedy, L.E. Limbird, J. Biol. Chem. 268 (1993) 8003–8011.
[7] B.F. O'Dowd, M. Hnatowich, M.G. Caron, R.J. Lefkowitz, M. Bouvier, J. Biol. Chem. 264 (1989) 7564–7569.
[8] R.D. Bramblett, A.M. Panu, J.A. Ballesteros, P.H. Reggio, Life Sci. 56 (1995) 1971–1982.
[9] J. Chen, H. Yang, A. Makriyannis, X.-Q. Xie, ICRS Meeting Symposium on the Cannabinoids, Hunt Valley, MD, vol. 7, 2000.

[10] P.H. Reggio, Curr. Med. Chem. 6 (1999) 665–683.
[11] E.P. Marin, A.G. Krishna, T.A. Zvyaga, J. Isele, F. Siebert, T.P. Sakmar, J. Biol. Chem. 275 (2000) 1930–1936.
[12] G. Choi, J. Landin, X.-Q. Xie, J. Pept. Res. 60 (2002) 169–177.
[13] S. Mukhopadhyay, H.H. McIntosh, D.B. Houston, A.C. Howlett, Mol. Pharmacol. 57 (2000) 162–170.
[14] B. Bechinger, Y. Kim, L.E. Chirlian, J. Gesell, J.M. Neumann, M. Montal, J. Tomich, M. Zasloff, S.J. Opella, J. Biomol. NMR 1 (1991) 167–173.
[15] H. Jung, R. Windhaber, D. Palm, K.D. Schnackerz, Biochemistry 35 (1996) 6399–6405.
[16] J.E. Johnson, R.B. Cornell, Mol. Membr. Biol. 16 (1999) 217–235.
[17] C. Altenbach, K. Cai, H.G. Khorana, W.L. Hubbell, Biochemistry 38 (1999) 7931–7937.
[18] O.P. Ernst, C.K. Meyer, E.P. Marin, P. Henklein, W.Y. Fu, T.P. Sakmar, K.P. Hofmann, J. Biol. Chem. 275 (2000) 1937–1943.
[19] P.L. Yeagle, C. Danis, G. Choi, J.L. Alderfer, A.D. Albert, Mol. Vis. 6 (2000) 125–131.
[20] M. Katragadda, J.L. Alderfer, P.L. Yeagle, Biophys. J. 81 (2001) 1029–1036.
[21] N. Greenfield, G.D. Fasman, Biochemistry 8 (1969) 4108–4116.
[22] M. Liu, X.-A. Mao, C. Ye, H. Huang, J.K. Nicholson, J.C. Lindon, J. Magn. Reson. 132 (1998) 125–129.
[23] P. Guntert, C. Mumenthaler, K. Wuthrich, J. Mol. Biol. 273 (1997) 283–298.
[24] D.J. Schibli, R.C. Montelaro, H.J. Vogel, Biochemistry 40 (2001) 9570–9578.
[25] H.W. Van Den Hooven, C.A. Spronk, M. Van De Kamp, R.N. Konings, C.W. Hilbers, F.J. Van De Van, Eur. J. Biochem. 235 (1996) 394–403.
[26] D. Palm, G. Munch, D. Malek, C. Dees, M. Hekman, FEBS Lett. 261 (1990) 294–298.
[27] R.E. Schreiber, E.R. Prossnitz, R.D. Ye, C.G. Cochrane, G.M. Bokoch, J. Biol. Chem. 269 (1994) 326–331.
[28] H. Shirai, K. Takahashi, T. Katada, T. Inagami, Hypertension 25 (1995) 726–730.
[29] K. Wakamatsu, A. Okada, T. Miyazawa, M. Ohya, T. Higashijima, Biochemistry 31 (1992) 5654–5660.
[30] T. Higashijima, J. Burnier, E.M. Ross, J. Biol. Chem. 265 (1990) 14176–14186.
[31] T. Higashijima, K. Wakamatsu, M. Takemitsu, M. Fujino, T. Nakajima, T. Miyazawa, FEBS Lett. 152 (1983) 227–230.
[32] H. Kusunoki, K. Wakamatsu, K. Sato, T. Miyazawa, T. Kohno, Biochemistry 37 (1998) 4782–4790.
[33] M. Han, V.V. Gurevich, S.A. Vishnivetskiy, P.B. Sigler, C. Schubert, Structure 9 (2001) 869–880.
[34] N.G. Abdulaev, K.D. Ridge, Proc. Natl. Acad. Sci. U. S. A. 95 (1998) 12854–12859.
[35] G.R. Marshall, R. Rango, G.M. Makara, R. Arimoto, O. Kisselev, Lett. Pept. Sci. 6 (1999) 283–288.